CCFE
CULHAM CENTRE FOR FUSION ENERGY

UK Atomic Energy Authority

UKAEA-CCFE-PR(18)73

A.V. Melnikov, E. Ascasibar, A. Cappa, F. Castejon, L.G. Eliseev, C. Hidalgo, P.O. Khabanov, N.K. Kharchev, A.S. Kozachek, L.I. Krupnik, M. Liniers, S.E.Lysenko, J.L. dePablos, V.N. Zenin, S.E. Sharapov, M.V. Ufimtsev and TJ-II team

Detection and investigation of chirping Alfven Eigenmodes with Heavy Ion Beam Probe in the TJ-II stellarator

Enquiries about copyright and reproduction should in the first instance be addressed to the UKAEA
Publications Officer, Culham Science Centre, Building K1/0/83 Abingdon, Oxfordshire, OX14 3DB, UK. The United Kingdom Atomic Energy Authority is the copyright holder.

Detection and investigation of chirping Alfven Eigenmodes with Heavy Ion Beam Probe in the TJ-II stellarator

A.V. Melnikov, E. Ascasibar, A. Cappa, F. Castejon, L.G. Eliseev, C. Hidalgo, P.O. Khabanov, N.K. Kharchev, A.S. Kozachek, L.I. Krupnik, M. Liniers, S.E.Lysenko, J.L. dePablos, V.N. Zenin, S.E. Sharapov, M.V. Ufimtsev and TJ-II team

This is a preprint of a paper submitted for publication in Nuclear Fusion

Detection and investigation of chirping Alfven Eigenmodes with Heavy Ion Beam Probe in the TJ-II stellarator

A.V. Melnikov[1, 2], E. Ascasibar[3], A. Cappa[3], F. Castejon[3], L.G. Eliseev[1], C. Hidalgo[3], P.O. Khabanov[1], N.K. Kharchev[1], A.S. Kozachek[4], L.I. Krupnik[4], M. Liniers[3], S.E.Lysenko[1], J.L. dePablos[3], V.N. Zenin[1], S.E. Sharapov[5], M.V. Ufimtsev[6] and TJ-II team[2]

[1] *National Research Centre "Kurchatov Institute", 123182, Moscow, Russia*
[2] *National Research Nuclear University "MEPhI", Moscow, Russia*
[3] *Fusion National Laboratory, CIEMAT, 28040, Madrid, Spain*
[4] *Institute of Plasma Physics, NSC KIPT, 310108, Kharkov, Ukraine*
[5] *CCFE, Culham Science Centre, Oxfordshire OX14 3DB, UK*
[6] *Department of Computational Mathematics and Cybernetics, Moscow State University, 119991, Moscow, Russia*

Alfven Eigenmodes were studied in low magnetic shear flexible heliac TJ-II (B_0=0.95 T, <R>=1.5 m, <a>=0.22 m) NBI heated plasmas (P_{NBI}≤1.1 MW, E_{NBI}=32 keV) by Heavy Ion Beam Probe (HIBP) [1, 2, 3]. The L-mode hydrogen plasma was investigated at various magnetic configurations with rotational transform $\iota(a)/2\pi = 1/q$ ~ 1.5 - 1.6. Co-, counter and balanced beam injection were explored. HIBP is capable to measure simultaneously the oscillations of the plasma electric potential, density and poloidal magnetic field. Earlier studies have shown the chirping modes with 250 kHz< f_{AE} <380 kHz at the low density $\bar{n}_e$ = $(0.3 – 1.5)\times10^{19}$ m^{-3} NBI heated plasmas with or without auxiliary ECR [3, 4]. Here we report the observation of the various types of the chirping modes, differs by frequency, radial location, amplitude and shape of the frequency dependence on time. Remarkably, the same mode may evolve, changing its type in the same frequency range in the single discharge. HIBP shows that location of the specific AE chirping may vary from ρ = 0 up to ρ = 0.8. The mode amplitude in potential varies from a few Volts up to 100 V. AEs are strongly affected by plasma current I_{pl}, e.g. caused by Ohmic heating coils. A variation of I_{pl} may even suppress the modes. Dual HIBP [5], consisting of the two HIBPs, separated at ¼ of the torus shows the high coherence between the plasma potential and density oscillations during the period of the frequency burst. The radial scan of the HIBP sample volume indicates the radial evolution of the potential and density perturbation during a single frequency burst of the chirping mode. Mean frequency of the chirping modes basically follow the model, based on the Alfven scaling and including actual iota evolution caused by I_{pl} changes [6].

1. Introduction

Alfvén Eigenmodes (AEs) induced by alpha-particles and fast ions created by auxiliary heating are capable to cause losses of the fast ions in magnetic fusion devices and in a future reactor [1]. Since that, the study of the AEs properties is one of the most reactor-relevant studies in the operating fusion devices. AE modes may exist in two basic forms. The first one is the steady frequency mode with a quasi-monochromatic character and the second one is chirping mode with a bursting amplitude and fast frequency change.

It is believed that chirping modes may affect fast ions in different way than more conventional steady frequency AE (convective vs diffusive transport). Estimations has shown that in ITER the diffusive losses of α-particles will be on the level of several percent (~5%), but the change the character of losses from diffusive to convective ones due to bursts of chirping modes may strongly increase the peak power of losses and exceed the tolerable level. Also chirping modes may promptly widen the α-particles heating power deposition profile that lead to undesirable oscillations of plasma column with frequency of chirping mode [2].

It was found that Electron Cyclotron Resonance Heating (ECRH) induces chirping modes in Neutral Beam Injection (NBI) heated plasma, see, for example, ASDEX Upgrade results [3]. In the low-density plasmas heated by NBI and ECRH in the TJ-II stellarator with low magnetic shear [4], AEs exist in the form of the chirping mode [5 – 7], while in the case of heating by NBI only and at a higher density, AEs with a steady frequency were observed [8 – 10]. The most pronounced steady modes were identified as Helicity induced Alfvén Eigenmodes (HAEs) and Global Alfvén Eigenmodes (GAEs) [10, 11]. Transitions between chirping and steady AEs were reported earlier for low-density plasmas ($0.5 < \bar{n}_e < 1.5\times10^{19}$ m^{-3}) heated by NBI and ECRH, and these transitions were found to depend on ECRH power, plasma density and the radial location of ECRH power deposition [5].

It was shown recently that the magnetic configuration has an essential effect on the frequency of the steady AEs [12]. Moreover, shot-to-shot magnetic configuration scans displayed in [6] showed a complex dependence of the chirping amplitude on the actual iota value.

The study of reference [12] has been extended to the non-linear AEs evolution and the results are presented in this paper, where the experimentally observed effects of a shot-to-shot magnetic configuration scans on the non-linear scenario of AEs evolution, namely on the transition from bursting to steady modes and vice versa is reported.

The aim of this study is to investigate the properties and location of the chirping modes in NBI plasmas on the TJ-II stellarator and to identify the conditions of the chirping – steady frequency AE transformation. The paper presents the results of the AEs studies with Heavy Ion Beam Probe (HIBP) measurements [13] supported by the AE monitoring with magnetic probes (MPs).

The new observation of the potential/density/B_{pol} oscillations associated to AEs are presented in the Section 3. Determination of the chirping mode radial location for NBI-only and NBI+ECRH plasmas are discussed in Section 4. The ECRH and iota effects on the chirping mode and the transition from chirping-to-steady mode are discussed in Sections 5–7. The results are summarized in Conclusions.

2. Experimental setup start from here

TJ-II is a four-period flexible heliac with low magnetic shear, and B_0=0.95 T, R_0=1.5 m, and $\langle a \rangle$=0.22 m. Most of the experiments were performed in the standard magnetic configuration denoted 100_44_64 (the numbers in this label refer to the currents in the magnetic field coils, $I_{CC}\_I_{HX}\_I_{VF}$, see figure 1 in Ref. [12] with vacuum rotational transform $\iota_{vac} = \iota/2\pi$ increasing from $\iota_{vac}(0)$=1.55 to $\iota_{vac}(a)$ = 1.65. Here I_{CC} is a current in the Circular Coil, I_{HX} in the Helical Coil and I_{VF} in the Vertical Field Coil. The coil currents in the configuration notation are shown in kA/10. ι_{vac} profile is shown in figure 1.

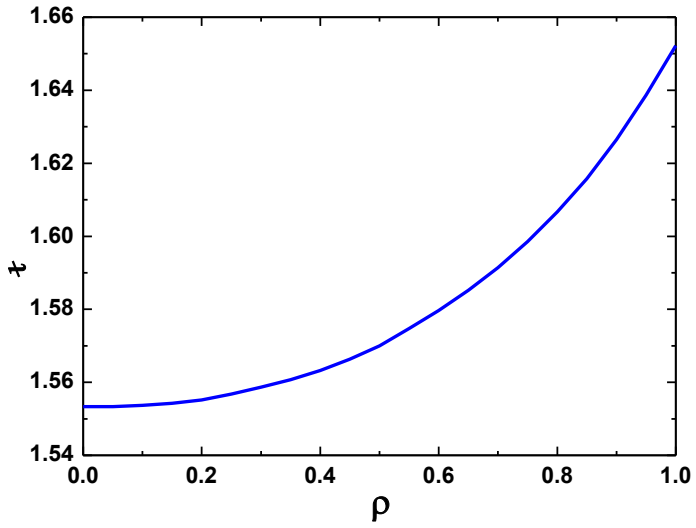

Figure 1. Vacuum rotational transform ι_{vac} profile in the standard configuration 100_44_64 of TJ-II.

The study was performed in the Hydrogen plasmas, which were formed and heated using one or two tangential Neutral Beam Injectors (NBI). One of them (Co-injector) has beam energy E_{NBI} =32 keV and deposited power P_{NBI} ~ 0.6 MW. It is directed along the toroidal magnetic field B_0. Another one is directed oppositely (Counter-injector) and it has beam energy E_{NBI} =29 keV and deposited power P_{NBI} ~ 0.45 MW. The beams have sub-Alfvénic velocity $V_{NBI} \sim 2.5\times10^6$ m/s, and $V_{NBI} \geq V_A/3$, where V_A is Alfvén velocity.

A typical discharge scenario is presented in figure 2(a). We see that in the considered L-mode discharges the line-averaged plasma density was kept at an almost constant relatively low level $\bar{n}_e \sim 0.6\times10^{19}$ m^{-3}, while central electron temperature was around 300 eV. Figure 2(b) shows the plasma density and temperature profiles against ρ, which is the magnetic surface flux label normalized to last closed magnetic surface radius. It is assumed that $\rho < 0$ for the High Field Side (HFS), and $\rho > 0$ the Low Field Side (LFS) of the plasma column. The low-density ($0.4 \leq \bar{n}_e \leq 1.0\times10^{19}$ m^{-3}) plasmas under studies are characterized by a broad T_e profile with $T_e(0)$ ~300–500 eV and flat T_i profile, $T_i(0)$ ~ 80 eV. At the same time, the electron density profile is generally parabolic, with rather flat core at $\rho <$ 0.4-0.5 and a sharp negative slope for $\rho >$ 0.5 [14].

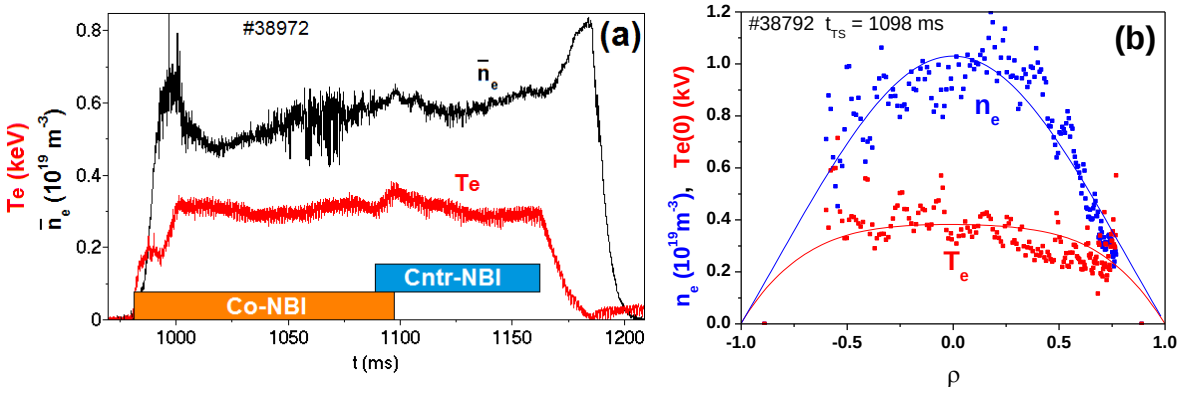

Figure 2. (*a*) The typical discharge scenario. Standard magnetic configuration 100_44_64, P_{CoNBI} = 0.59 MW; $P_{CntrNBI}$ = 0.43 MW; (*b*) the density and temperature profiles measured by Thomson Scattering at t = 1098 ms are shown with symbols; solid lines show the fitting curves.

TJ-II is equipped with a poloidal array of 24 magnetic or Mirnov probes (MP) placed inside the vacuum vessel for measuring magnetic perturbations [15]. In addition to the MP diagnostics, we employed the Thomson Scattering diagnostics, providing the density and T_e profiles once per shot and (HIBP) [16, 17]. HIBP was recently used to study quasicoherent modes [18–20] and specifically for Alfvén Eigenmodes [8–10]. HIBP provides simultaneously local internal information about three parameters: electric potential and density profiles and oscillations, and also poloidal magnetic field oscillations [8–10]. This diagnostic tool could thus provide internal amplitudes of AEs. Although the HIBP diagnostic tools on TJ-II were described in [16, 17], it is worthwhile to mention here some relevant details. HIBP operates with Cs^+ primary ions having initial energy E_b = 125 keV. HIBP provides measurements of the local plasma potential φ_{pl}^{SV} in a sample volume (SV), which is proportional to the secondary beam energy

$$\varphi_{\mathrm{pl}}^{\mathrm{SV}} = (E_{\mathrm{d}} - E_{\mathrm{b}}) / e, \qquad (1)$$

where E_d is an energy of the secondary ions Cs^{++} leaving the plasma after their ionization in the sample volume. The local plasma density $n_{\mathrm{e}}^{\mathrm{SV}}$ in the sample volume is proportional to the secondary beam intensity I_{tot}

$$I_{tot}(\rho,t) = 2I_b n_e^{SV}(\rho,t)\sigma^{12}\lambda \times \exp\left(- \int\limits_{L_1(\rho)} n_e(s)\sigma^{12}(s)ds - \int\limits_{L_2(\rho)} n_e(s)\sigma^{23}(s)ds \right) \qquad (2)$$

where I_b is the intensity of the primary probing beam, σ^{12} and σ^{23} are the effective cross-section for electron impact ionization for primary and secondary ions, λ is the length of the sample volume. The integrals are taken along the primary L_1 and the secondary L_2 trajectories in the plasma and describe the primary and secondary beams attenuation. The poloidal magnetic field B_{pol} creates a toroidal force component affecting the beam trajectory due to the Lorenz force.

$$m\frac{\partial \vec{V}}{\partial t} = Ze\left[\vec{V} \times \vec{B}\right] \qquad (3)$$

Here V is the probing particle velocity, m is its mass, B is the total magnetic field. Toroidal force component results in the appearance of a toroidal velocity component of the beam along the trajectory. Thus, the poloidal field B_{pol} and its fluctuations may be retrieved from toroidal velocity $V_{\zeta \mathrm{d}}$ and displacement ζ_{d} of the probing beam in the detector using the integral relations [8]. The HIBP sample volume (SV) size determines the spatial resolution ~1

cm. SV radial position ρ_{SV} can be varied over the whole plasma column, $-1 < \rho_{SV} < 1$, of TJ-II [21].

For the considered low-density plasmas the I_{tot} mean (time-averaged) radial profile is symmetric LFS-HFS. On top of that, I_{tot} increases with line-averaged density $\bar{n}_e$ up to $\bar{n}_e \leq 1.3\times10^{19}$ m^{-3} due to the local density raise in SV. So, the local term, representing the local density perturbations in SV $\tilde{n}$ dominates in $\tilde{I}_{tot}$ in both LFS-HFS [Last TJ-II paper 2016]. The same holds for ζ_d , which is indeed proportional to $\tilde{B}_{pol}$ in a sample volume [Last TJ-II paper 2016]. Potential perturbation measurements are intrinsically local.

3. Chirping mode observation in the core NBI plasma

In TJ-II chirping modes are typically observed in the low-density NBI discharges with and without auxiliary ECRH [Jimenez-Gomez 2011, Melnikov 2014]. This study is dedicated to NBI-sustained plasmas. An example of AE bursts is presented in figure 3. Figure shows an example of the mode with a mean frequency around 300 kHz, which lasts about 100 ms. Due to the Lithium coating of the TJ-II vacuum vessel, the plasma density is under effective control, i.e. low-density NBI discharges are stable and reproducible. Figure presents an example of the very interesting and beautiful phenomenon: long-lasting chirping mode, with smoothly evolving chirping pattern. The top box (a) of the figure presents this high-frequency chirping mode, as observed by Mirnov Probe (MP). The lower boxes show this mode as observed by HIBP parameters (density (b), potential (c), and B_{pol} (d) in the scanning mode of HIBP operation. Bursts with the fast frequency sweep as large 50 kHz (frequency chirping) were observed in the TJ-II plasma for the first time by HIBP. The typical burst period in TJ-II is about 1-2 ms, while the burst 'lifetime' (time from burst appearance to the burst vanishing) is twice shorter. The HIBP radial scan lasts 10 ms, so HIBP observes 4-5 chirpings when SV passes through plasma diameter from LFS to HFS and back.

Figure presents several different chirping pattern marked by red ovals on the figure 3 a). One may see that each pattern is visible in the same way in all four parameters, presented in the figure. The patterns of the figure 3 are presented in more details in figure 4. Figure 3 shows that the evolution of the patterns is really smooth, the wave-particle interactions process is continuous, non-interrupted. Figure 3 (e) shows the plasma density profile evolution, as measured by intensity of the secondary beam I_{tot}. The mean density and the profile as well exhibit really tiny changes, the similar tiny changes are visible in the total plasma current I_{pl}, as shown in Figure 3 (f), so rotational transform iota has small changes. It

is suggested that these small evolution of I_{pl} and density profile caused the evolution of the chirping mode pattern.

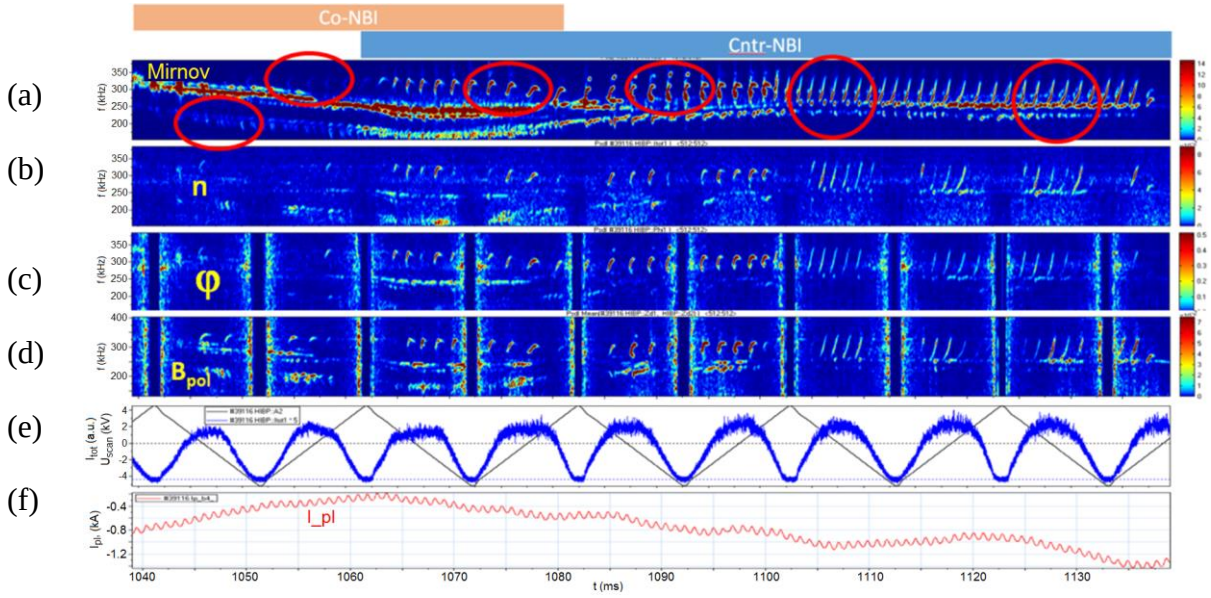

Figure 3. Chirping pattern evolution in a single shot, as observed by Mirnov Probe (*a*), HIBP density (b), HIBP potential (c) and HIBP B_{pol} (d). HIBP operates in the scanning mode, scanning voltage U_{scan} (t) is shown in black in (e), it represents ρ_{SV} (t), periodically changed from -1 to 1, blue curve in (e) – shows the sequence of density profiles, obtained in each scan, (f) – plasma current, measured by Rogowski coil. Shot #39116 with standard magnetic configuration 100_44_64.

The difference in the pattern reflects the fine features of the wave-particle interactions resulting in chirping mode excitation. Figures 3 and 4 shows that these features are very sensitive to the tiny changes of iota and density profile.

4. Radial expansion of the chirping mode

Radial scan of HIBP Sample Volume is an effective tool to study AE location [X, Y]. An application of this method to the chirping mode with large frequency bursts is shown in the figure 5. Top box shows the power spectrogram of the density (I_{tot}) perturbation, showing a pronounced chirping mode with raising frequency. The lower box shows the radial evolution of the SV, ρ_{SV} (t).

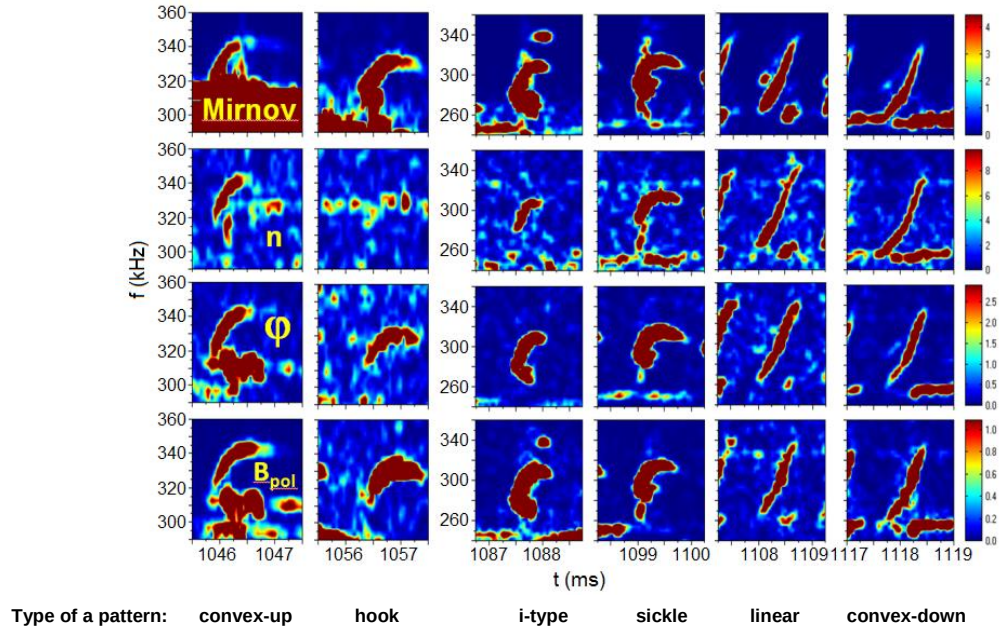

Figure 4. Multiple chirping pattern observed in a single shot. Data are taken from figure 3 with the same notation.

One may see that the image of the individual burst of the mode is not the same for evolving ρ_{SV} , for larger $|\rho_{SV}|$ the burst, visible by HIBP, starts with higher frequency then for smaller one. Figure shows that this observation does not depend on the direction of the ρ_{SV} changing, if it increases or decreases.

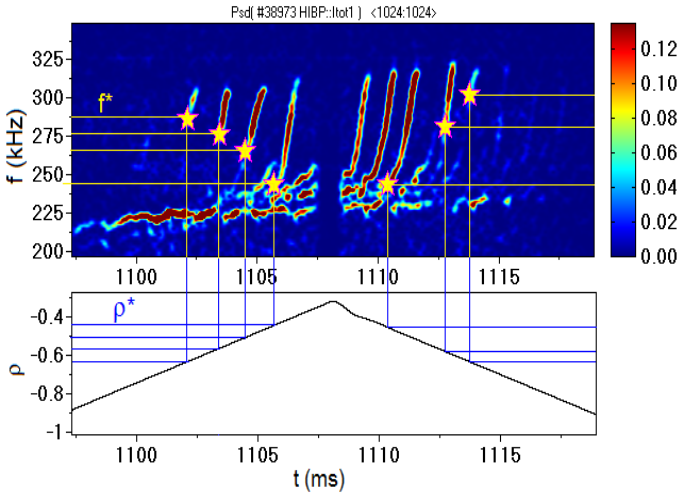

Figure 5. Observation of the chirping-up AE modes by HIBP radial scan. Stars denote the time instants of the start of the observation of the burst. Yellow lines shows the starting frequencies f^*, while blue lines show corresponding normalized radius ρ^* . Both directions of scan are shown. #38973, configuration 100_42_64, convex-down-type mode.

At the same time the image of the mode in the Mirnov Probes is the same for all bursts, showing frequency raise from permanent minimum to permanent maximum.

Figure 5 defines the starting frequency of burst f^* and the corresponding starting normalized radius ρ^*. ρ^* has a meaning of a radial outer frontier, inside which the chirping-up mode starts with lowest frequency f^*. The dependence of the ρ^* on the frequency f^* is shown on the figure 6. It collects the points from several successive scans on the spectrograms of plasma potential and density.

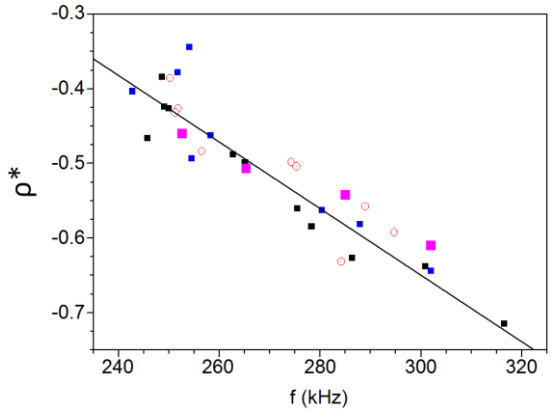

Figure 6. Dependence of the outer radial frontier of the chirping-up AE mode on starting frequency of the burst f^*, obtained by HIBP radial scan.

Figure 6 shows that for chirping-up AE mode outer bound ρ^* linearly increases or expands outwards with low-limit chirping frequency, as determined by several HIBP scans. At the same time, the inner bound, which corresponds to the high frequency limit of the burst remains almost unchanged.

Figure 7 shows the spectrograms of potential (a) and density (b) with radial reconstruction of the bounds of the bursts by presenting ρ^* as a function of time for each burst (c). The boxes (a) and (b) shows the similarity of the typical image of the chirping mode by HIBP scan for plasma potential and density, which is similar to Figure 5. Power spectrogram of Mirnov Probe (*d*) shows that for the mode under study all bursts are same, showing frequency raise from minimum to maximum. Box (c) presents the interpretation of the observations, shown in Figures 5 and 6. Here pink color shows the area of existence of the bursts, which lies between periodically variating lower bound ρ^* and permanent upper bound. The mode under study is chirping-up mode, so each burst starts from f^* and it reaches the highest frequency at the permanent upper radial bound. This means that the burst originates in the core region and then with the frequency raise it expands in radius towards the edge,

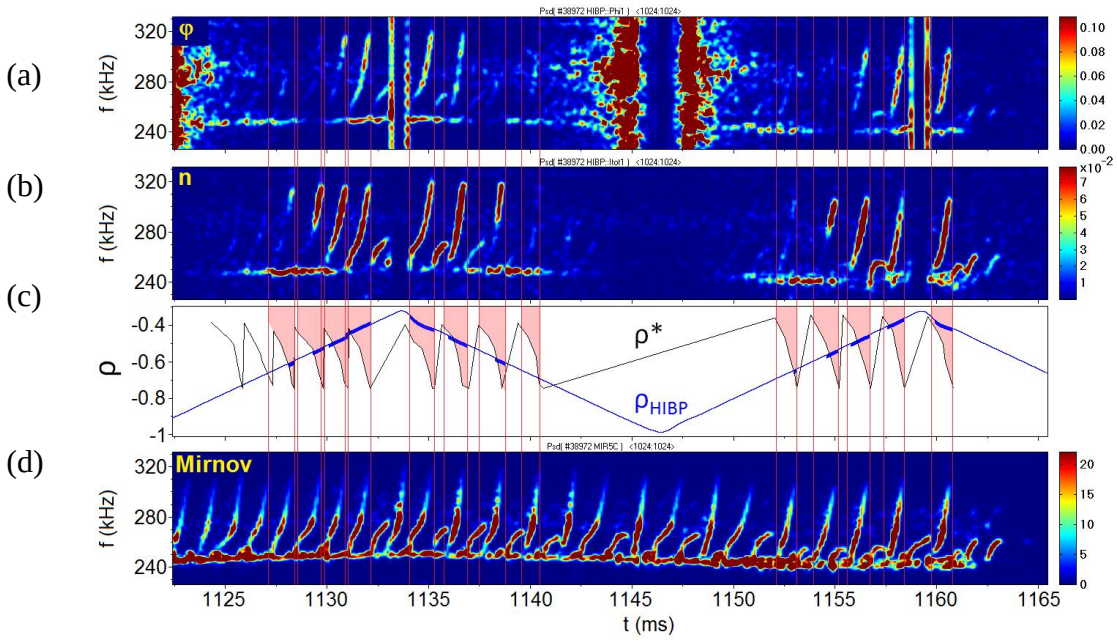

Figure 7. Chirping and HIBP scan: schematic explanation. Power spectral density evolution for HIBP potential (*a*), HIBP density (*b*), blue curve in (*c*) represents ρ_{SV} (t), periodically changed from -1 to -0. 35 in HIBP scanning mode, (*d*) power spectrogram of Mirnov Probe. Pink color in (*d*) denotes the time-spatial evolution of the area of existence of the bursts, which is limited by lower bound ρ^*, marked by black curve, which increases in time up to the upper bound. Fat blue lines shows the intersection of this area with ρ_{SV} (t), representing the localization of the frequency area from starting frequency of burst f^* to the final maximum frequency of burst. Shot #38972 with standard magnetic configuration 100_44_64, convex-down-type mode evolving to linear-type mode.

remaining in the birth area. Near the burst origin local HIBP observes the whole frequency burst, while near the edge it only observes the upper part of the frequency burst.

7. Discussion

The radial expansion of the bursts takes place at the area of the density gradient. Unless the TS data has large uncertainties for the considered low-density plasma, which are in the range of 0.1[1019, it can be estimated the density decay from the inner bound of the mode (r=0.4) to the outer bound of the mode (r=0.7) as a factor of 2 decay. According to the Alfven law, the mode frequency for the low density in the outer bound should be in a factor of sqrt (2) higher than at the origin. This estimated frequency coincides with the observations within

the experimental accuracy of the frequency measurements, which is around 10 kHz. So, the observation may be interpreted as follows: the mode under study originates near r=0/4 and then expands outwards, encountering the frequency increase due to decay of the density in the area of expansion.

8. Conclusions

HIBP observation shows the new important features of the chirping Alfven Eigenmodes in the low-density NBI discharges of TJ-II. The pattern of the chirping-up mode may evolve during a single discharge with only tiny variation of plasma density and rotational transform. There are up to six various types of the chirping pattern found. During individual frequency burst the density and plasma potential perturbation area expands outwards for the considered chirping-up mode. The frequency raise is in line with the density decay in the area of expansion.

References

[1] Heidbrink W.W. *et al* 2008 *Phys. Plasmas* **15** 055501
[2] Gryaznevich M.P. *et al* 2008 *Nucl. Fusion* **48** 084003
[3] Garcia-Munoz M. *et al* 2015 Impact of localized ECRH on NBI driven Alfvén eigenmodes in the ASDEX Upgrade tokamak. (*Proc.42nd EPS Conf. Plasma Physics, Lisbon, 22 - 26 June 2015*) P1.148 http://ocs.ciemat.es/EPS2015PAP/html/
[4] Ascasibar E. *et al* 2002 *Plasma Phys. Control. Fusion* **44** B307
[5] Nagaoka K. *et al* 2013 *Nucl. Fusion* **53** 072004
[6] Cappa A. *et al* 2014 Influence of ECR Heating on NBI-driven Alfvén Eigenmodes in the TJ-II Stellarator (*Proc. 25th IAEA Fusion Energy Conf., St. Petersburg, Russia*, *13–18 October 2014*) EX/P4-46 http://www-naweb.iaea.org/napc/physics/FEC/FEC2014/fec_sourcebook_online.pdf
[7] Melnikov A.V. *et al* 2016 *Nucl. Fusion* **56** (2016) 076001
[8] Melnikov A.V. *et al* 2010 *Nucl. Fusion* **50** 084023
[9] Jiménez-Gómez R. *et al* 2011 *Nucl. Fusion* **51** 033001
[10] Melnikov A.V. *et al* 2012 *Nucl. Fusion* **52** 123004
[11] Melnikov A.V. *et al* 2011 *Plasma and Fusion Research* **6** 2402030
[12] Melnikov A.V. *et al* 2014 *Nucl. Fusion* **54** 123002
[13] Dnestrovskij Yu.N. *et al* 1994 *IEEE Trans. Plasma Sci*. **22** 310
[14] Hidalgo C. *et al* 2005 *Nucl. Fusion* **45** No 10 S266-S275
[15] Jiménez-Gómez R. *et al* 2007 *Fusion Sci. Technol.* **51** 20
[16] Donné A.J.H. *et al* 2002 *Czech J. Phys.* **55** 1077
[17] Bondarenko I.S. *et al* 2001 *Rev. Sci. Instrum*. **72** 583
[18] Melnikov A.V. *et al* 2011 *Nucl. Fusion* **51** 083043
[19] Fujisawa A. *et al* 2007 *Nucl. Fusion* **47** S718
[20] Melnikov A.V. *et al* 2006 *Plasma Phys. Control. Fusion* **48** S87.
[21] Melnikov A.V. *et al* 2007 *Fusion Sci. Technol.* **51** 31
[22] Ross D.W. *et al* 1992 *Rev. Sci. Instrum*. **63** 2232
[23] Fujisawa A. 1997 *Rev. Sci. Instrum*. **68** 3393
[24] Simcic V.J. *et al* 1993 *Phys. Fluids B* **5** 1576
[25] Zhang C., Zhang W., Zhihong L. and Li D. 2013 *Phys. Plasmas* **20** 052501